J. Astrophys. Astr. (2008) **29,** 125–145

X-ray Emission from Solar Flares

Rajmal Jain, Malini Aggarwal & Raghunandan Sharma
Physical Research Laboratory, Department of Space, Government of India, Navrangpura, Ahmedabad 380 009, India.

Abstract. Solar X-ray Spectrometer (SOXS), the first space-borne solar astronomy experiment of India was designed to improve our current understanding of X-ray emission from the Sun in general and solar flares in particular. SOXS mission is composed of two solid state detectors, *viz.*, Si and CZT semiconductors capable of observing the full disk Sun in X-ray energy range of 4–56 keV. The X-ray spectra of solar flares obtained by the Si detector in the 4–25 keV range show evidence of Fe and Fe/Ni line emission and multi-thermal plasma. The evolution of the break energy point that separates the thermal and non-thermal processes reveals increase with increasing flare plasma temperature. Small scale flare activities observed by both the detectors are found to be suitable to heat the active region corona; however their location appears to be in the transition region.

Key words. Solar flares—X-ray detectors—X-ray line emission and continuum—break energy—microflares.

1. Introduction

The Solar X-ray Spectrometer (SOXS) mission (Jain *et al.* 2000a, 2000b, 2005, 2006a, b) was launched onboard an Indian geostationary satellite namely GSAT-2 on 8 May 2003 by GSLV-D2 rocket. The SOXS aims to study the high energy and temporal resolution X-ray spectra from solar flares. The SOXS consists of two independent payloads, *viz.*, SOXS Low Energy Detector (SLD) and SOXS High Energy Detector (SHD) payloads. The SLD is comprised of two semiconductor devices, *viz.*, Silicon PIN detector for 4–25 keV (area 11.56 mm^2); and Cadmium Zinc Telluride (CZT) detector for 4–56 keV energy range (area 25 mm^2). These state-of-the-art solid state detectors in SLD operate at near room temperature, i.e., at -20°C. Both detectors have 100 ms temporal resolution characteristics, which make them most appropriate for solar flare research in context to energy transport and acceleration time scales of particles. The energy resolution revealed by Si PIN detector is sub-keV. The SLD payload is designed and developed at the Physical Research Laboratory in collaboration with ISRO Satellite Centre (ISAC), Bangalore, and Space Application Centre (SAC), Ahmedabad.

The X-ray energy spectrum from a typical large solar flare is dominated by soft X-ray line and thermal (free-free) bremsstrahlung emission at $\varepsilon \approx$ 1–20 keV, and collisional bremsstrahlung of non-thermal electrons at $\varepsilon \approx$ 20–1000 keV (Jain *et al.* 2000a, 2000b; 2005). The measurements of soft X-ray flux before and during the flare provide a wonderful opportunity to study the soft X-ray characteristics of active region

corona. The high sensitivity of the SLD and sub-keV energy resolution of Si PIN detector allows measuring of the intensity and mean energy of the Fe and Fe/Ni line features at approximately 6.7 and 8 keV respectively (Phillips 2004; Jain *et al.* 2005, 2006b; Phillips *et al.* 2006) as a function of time in all classes of flares. The Fe-line complex is due mostly to the 1s-2p transitions in He-like and H-like iron, FeXXV and FeXXVI respectively, with associated satellite lines. The weaker Fe/Ni line feature at $\sim$ 8 keV made up of emission from He-like nickel and more highly excited FeXXV ions is also evident in the more intense flares (Phillips 2004; Phillips *et al.* 2004).

The detailed investigation by Jain *et al.* (2006b) of X-ray spectra of M-class flares observed by Si detector of SLD showed that peak energy and equivalent width (w) of Fe line feature vary as a function of temperature of flare plasma. Further, they also showed that the whole energy spectrum of 4–20 keV cannot be fitted with single temperature approximation. They used two temperatures to obtain the best fit for line emission and continuum. The equivalent width of the Fe-line feature was observed to exceed the theoretical one in the temperature range of $\approx$ 20–60 MK, which could indicate multi-thermal flare plasma or higher iron abundance. The ratio of the 6.7 keV Fe to the 8.0 keV Fe/Ni line fluxes is therefore expected to decrease progressively with higher plasma temperature (Phillips 2004).

The collisional bremsstrahlung produced by non-thermal electrons in many flares found to be very strong over thermal bremsstrahlung, and their contribution vary over-flare duration showing the break in the energy spectrum. However, in view of our currently poor knowledge of low energy cut-off of collisional bremsstrahlung we are not able to estimate precisely the number of electrons that participated in non-thermal X-ray emission. On the other hand, the poor spectral resolution of X-ray detectors put a constraint to measuring precisely the break energy point between thermal and non-thermal contributions. The improved energy resolution of sub-keV and 1.7 keV of Si and CZT detectors respectively in their dynamic energy range over the earlier detectors provide an opportunity to measure the break energy point more convincingly.

The heating of solar corona is a long enduring problem in solar physics and many investigators have proposed micro and nanoflares as potential candidates for heating the active region corona. Both Si and CZT detectors of SOXS mission have observed a large number of small scale flare activity during the last four years. The signatures of Fe-line feature emission in micro flares as evident by Si and CZT detectors support the concept of small scale flares as a source of coronal heating.

Therefore, the purpose of this paper is to present the potentialities of Si and CZT detectors of SOXS mission in context to quantifying X-ray emission characteristics of solar flares in general, and improving our current understanding of thermal and non-thermal mechanisms and the role of microflares in heating the active region solar corona in particular.

2. Observations

2.1 *Instrumentation*

The instrumentation of the SLD payload, its in-flight calibration and operation has been described by Jain *et al.* (2005, 2006a, 2006b). The SLD payload is functioning satisfactorily onboard the GSAT-2 spacecraft and so far more than 450 flares of importance greater than GOES C1.0 have been observed. The SLD is comprised of two

semiconductor devices, viz., Silicon PIN detector for 4–25 keV (area 11.56 mm^2); and Cadmium Zinc Telluride (CZT) detector for 4–60 keV energy range (area 25 mm^2). The spectral resolution revealed by Si detector is 0.7 keV @ 6 keV and 0.8 keV @ 22.2 keV, which is better over the earlier detectors used for solar flare research in this energy range. However, the spectral resolution of CZT detector is 1.7 keV throughout its dynamic energy range of 4–56 keV. Further their temporal resolution capabilities are also superb, however, we designed for 100 ms during flare mode in order to achieve feasible energy spectrum. The operating temperature of both detectors in the range -5 to -30°C is achieved using thermoelectric cooler that coupled with the detector. The detector package is mounted on a Sun Aspect System which keeps the Sun in the center of the detector for an interval between 03:55 and 06:30 UT everyday. However, after 06:30 UT, the temperature on the detectors exceeds the limit to cool down by thermoelectric cooler. Thus SLD payload provides uninterrupted data for $\sim$ 2.5 h everyday. The SLD data are of two types: temporal mode (light curves) and spectral mode. The in-flight tests and onboard calibration of the detectors were successfully carried out between 22 May and 6 June 2003.

2.2 *Dataset*

The temporal data, i.e., intensity (counts/s) as a function of time is revealed in four energy bands, viz., 6–7 keV (L1), 7–10 keV (L2), 10–20 keV (L3) and 4–25 keV (T) by Si detector, while in five energy bands by CZT detector viz., 6–7 keV, 7–10 keV, 10–20 keV, 20–30 keV and 30–56 keV. We selected flares of *GOES* importance class B, C and M for the current study of different objectives as described in the text.

2.3 *Temporal and spectral evolution*

In Fig. 1, we show the temporal evolution of 14 August 2004 and 27 July 2005 flares made from the spectral data of the Si and CZT detectors. The time resolution for spectral mode observations during quiet period is 3 s but during flare mode it is 100 ms, which however, is restricted to 287.5 s only in view of telemetry constraints. The intensity (counts/cm^2/s/keV) of the light curves is shown in 4.1–10, 10–15 and 15–25 keV bands from Si detector, while in 25–35 and 35–55 keV bands from CZT detector. It may be noted that the 14 August 2004 flare is rising in the beginning as a slow heating of the plasma, and then impulsive transport followed by long enduring thermal component, while the 27 July 2005 flare is a gradual long enduring flare. The onset of flare is delayed in higher and higher energy channels but peaks earlier than previous bands, which suggests that radiative cooling is the dominant mechanism in cooling the flare plasma.

The spectral evolution of these two flares is shown in Fig. 2. The low intensity below 6 keV is due to aluminum plus kapton filter mounted on the detector head to cut the X-ray photons up to 4 keV and electrons up to 300 keV falling in the line-of-sight of the detector. It may be noted that the Fe and Fe/Ni lines are unambiguously visible in the count spectra at $\sim$ 6.7 and $\sim$ 8 keV respectively, however their intensity and width vary over time. The count spectra are de-convoluted over the instrumental response to obtain the photon spectra.

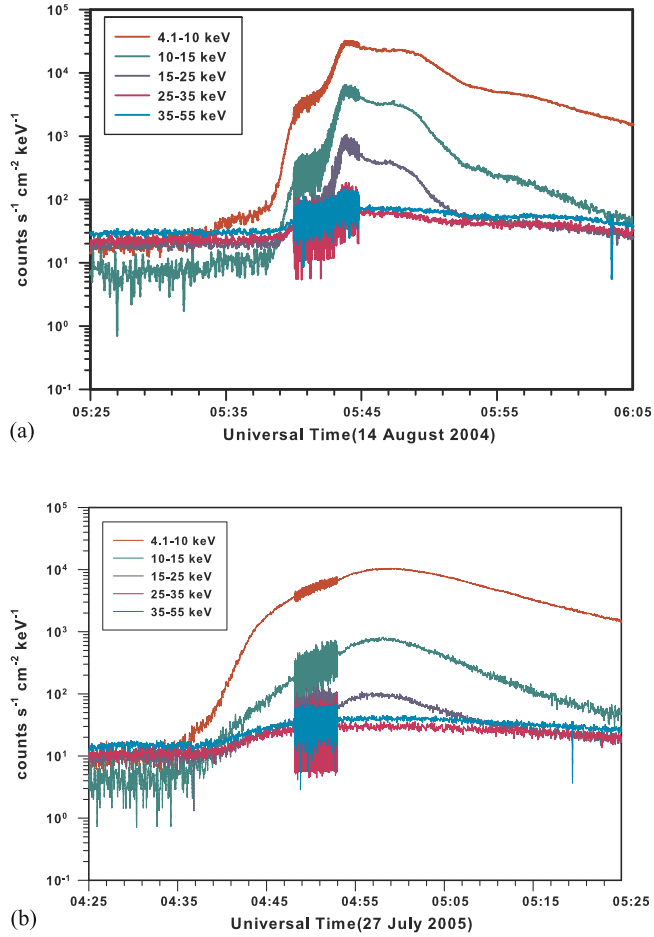

Figure 1(a & b). Light curves of the 14 August 2004 and 27 July 2005 solar flares as recorded by Si and CZT detectors of SLD/SOXS mission. 100 ms cadence during flare mode may be noted.

3. Analysis and results

We use the OSPEX (Object Spectral Executive) software package inside SolarSoft to analyse the data. The OSPEX is an object-oriented interface for X-ray spectral analysis of solar data. It is the next generation of SPEX (Spectral Executive) written by R. Schwartz in 1995. Through OSPEX, the user reads and displays the input data, selects and subtracts background, selects time intervals of interest, selects a combination of photon flux model components to describe the data, and fits those components to the spectrum in each time interval selected. During the fitting process, the response matrix is used to convert the photon model to the model counts to compare with the input count data. The resulting time-ordered fit parameters are stored and can be displayed and analyzed with OSPEX. The entire OSPEX session can be saved in the form of a script and the fit results stored in the form of a FITS file.

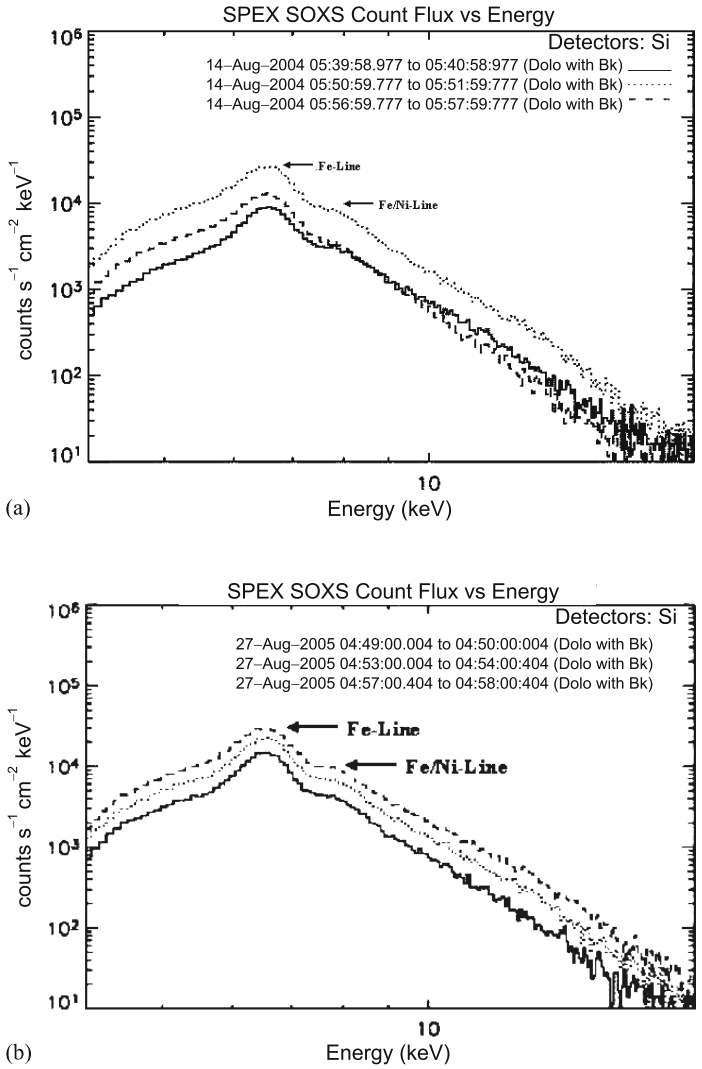

Figure 2(a & b). Spectral evolution of the 14 August 2004 and 27 July 2005 flares. The X-ray flares intensity (counts/cm^2/s/keV) at three different intervals of time is shown as a function of energy. Fe and Fe/Ni line features are marked on the spectrum.

The OSPEX subroutines have been updated to undertake detailed temporal and spectral data analysis of Si and CZT detectors of SLD/SOXS mission. The raw data for spectral mode observations was first corrected for any spurious or false flare as well as for pre-flare background. The spectrum at a given time is made by integrating the spectra over an interval of 60 s period. The OSPEX enables us to look at the temporal evolution, spectrogram and spectral evolution. It also enables us to fit energy spectra using CHIANTI codes (Dere *et al.* 1997) for flare plasma diagnostics with the application of various thermal, line emission, multi-thermal, and non-thermal functions.

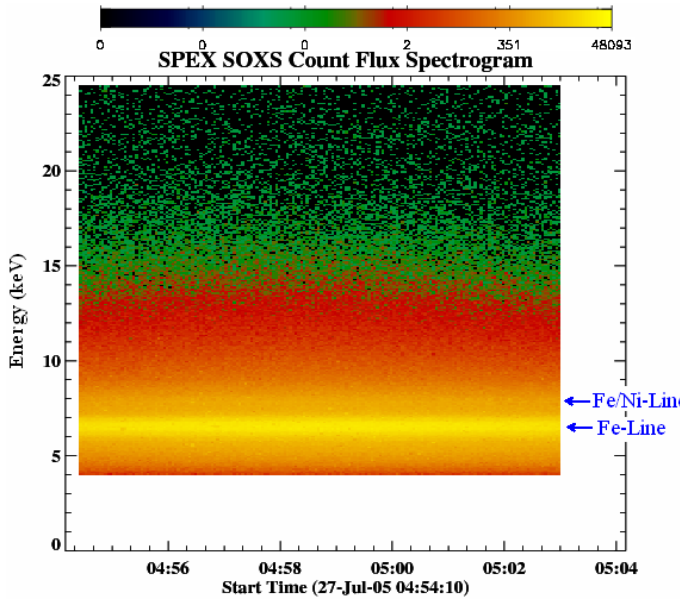

Figure 3. The spectrogram showing variation of Fe and Fe/Ni line features as a function of time during the flare of 27 July 2005.

3.1 *X-ray emission from Fe line and Fe/Ni lines*

In order to study the Fe and Fe/Ni line emission it is rather more important to study their evolution with the flare development, i.e., as a function of temperature because the line emission and its intensity vary with temperature and emission measure (Phillips 2004). It may be noted from Fig. 2 that the peak intensity, peak energy and area under the curve of the lines vary over time. In fact the plasma temperature and hence emission measure vary over time and these factors mainly control the shape of the line. The non-thermal contribution also plays a role and therefore needs to be considered as an important parameter including temperature and emission measure.

The Fe line feature is here defined as the excess above the continuum, as observed by Si spectrometer with spectral resolution (FWHM) $\leq$ 0.7 keV, in the energy range 5.8–7.5 keV, and similarly the Fe/Ni line feature in the range 7.5–9.2 keV (Phillips 2004, Jain *et al.* 2006b). It may be noted from the flare spectrogram shown in Fig. 3 that the Fe and Fe/Ni features including the peak energy and intensity vary over the flare evolution, which suggests that the abundance and centroid/peak energy of the emission line vary as a function of temperature.

We analyzed 32 and 45 spectra of 14 August 2004 and 27 July 2005 flares respectively. We use forward fitting program in OSPEX to fit the count spectra where instrumental response matrix for Si and CZT detectors is incorporated. The important aspect of our spectra-fit analysis is consideration of multi-thermal power-law function, which assumes differential emission measure (DEM), in addition to line emission function, and non-thermal power-law function in order to estimate the contribution of non-thermal electrons in the flare plasma. The DEM in the multi-thermal power-law is of the following form:

$$\mathrm{DEM}(T) = a_0 \cdot \left(\frac{2}{T}\right)^{\gamma_{MT}}, \tag{1}$$

where a_0 is differential emission measure at temperature $T = 2\,\mathrm{keV}$ in units of $10^{49}\,\mathrm{cm}^{-3}\,\mathrm{keV}^{-1}$ and γ_{MT} is power-law index for calculating the differential emission measure at the temperature T obtained from multi-thermal power law fit of the observed spectrum.

The multi-thermal power-law function enables us to measure the emission measure, the minimum (assumed 5.8 MK) and maximum temperature of the flare plasma, power-law index and the abundance of Fe-line relative to corona. The line emission Gaussian function provides integrated intensity, centroid energy of the line and line width. On the other hand, the non-thermal function allows us to measure power-law index below and above break energy. In Fig. 4, we show a typical example of count spectra-fit with the application of the above functions.

It may be noted from Fig. 4 that non-thermal bremsstrahlung also contributes considerably to the evolution of Fe and Fe/Ni line features in addition to significant

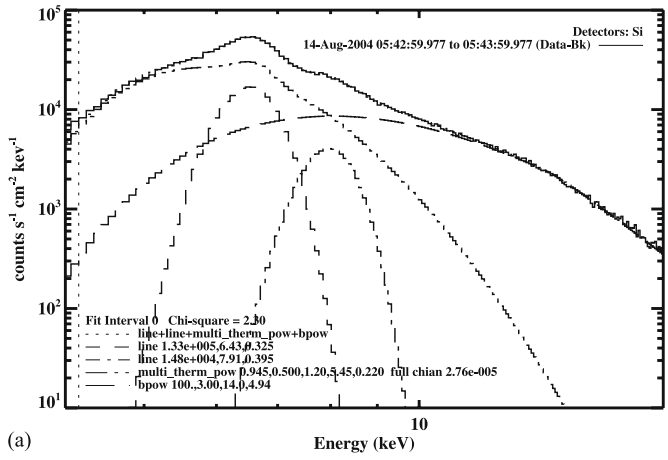

Figure 4. (*Continued*)

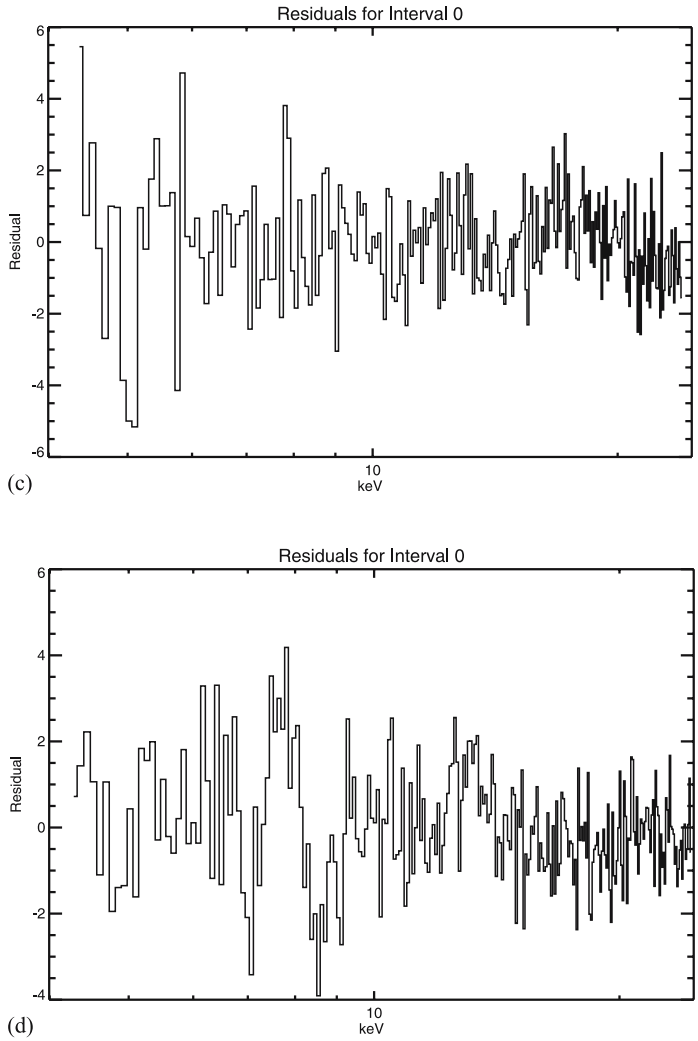

Figure 4(a–d). Fit count spectra **(a & b)** observed near peak time of 14 August 2004 and 27 July 2005 flares considering line Gaussian, multi-thermal and broken power-law functions using Chianti codes. Residuals as a function of energy for the fit spectra are also shown in **(c)** and **(d)**.

contribution by thermal processes inside the flare plasma. Once the count spectrum is fitted, it can be de-convoluted over the instrumental response to obtain the photon spectrum which is generated using the fitted model count spectrum. We do not use the pulse piled up spectra for analysis to avoid false temperature results. To obtain a reasonably satisfactory model fit to the count spectra we fit the parameters taking in consideration the following conditions:

- Parameters should give satisfactory values for the reduced chi-squared ($\chi^2 < 3$).
- The temperature and emission measure should have a consistent time history, i.e., their variation should not be very large from one to the next spectra.

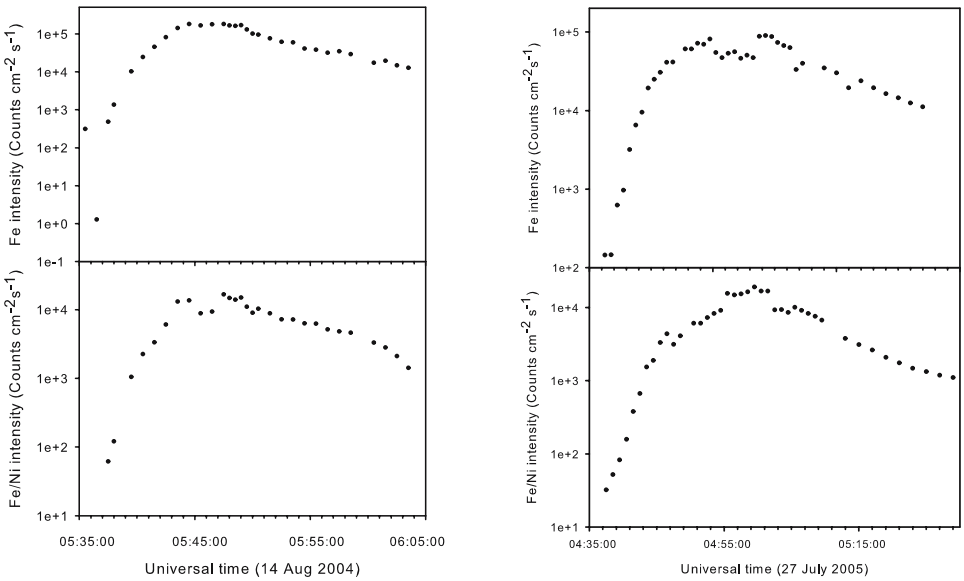

Figure 5. The intensity of Fe and Fe/Ni line features varying over time in 14 August 2004 and 27 July 2005 flares.

In Fig. 5, we show the integrated line intensity variation of Fe and Fe/Ni line features as a function of time measured in 14 August 2004 and 27 July 2005 flares. It may be noted that the line intensity follows by and large the flux intensity of the flare in 4–10 keV. However, line intensity of Fe and Fe/Ni features is found to increase as a function of temperature measured in these two flares as shown in Fig. 6. It may be noted that the increase in the intensity of the line feature with temperature is exponential up to 25 MK and then it remains to almost the same level until $\sim$ 80 MK. Based on the analysis of more than 10 flares, Jain *et al.* (2006a) showed that equivalent width (abundance) of Fe line feature increases exponentially up to 25 MK and remains stable up to 45 MK. However, it reduces with temperature exceeding 45 MK. Perhaps, a similar result may be observed if analysis were conducted for large number of flares.

3.2 *X-ray emission from flare plasma*

In Fig. 7, we show the variation of flux in 10–20 keV, temperature and emission measure over time for these two flares of 14 August 2004 and 27 July 2005. It may be noted when temperature of the flaring plasma is decreasing the emission measure is increasing.

If the flare is dominated by thermal emission mechanism then evolution of flux follows the evolution of temperature as may be noted in the case of 27 July 2005 flare (cf. Fig. 7 – right side). On the contrary, at the onset of the 14 August 2004 flare, temperature is not high rather DEM is very high and remains between 10^{47} and 10^{50} cm^3 $\cdot$ keV^{-1} during rise phase. This suggests that non-thermal bremsstrahlung was the principal mechanism for onset of the flare, which perhaps was generated by acceleration of particles causing the large ionization, and hence producing very high electron density revealed by large DEM. We estimated volume of the flare from

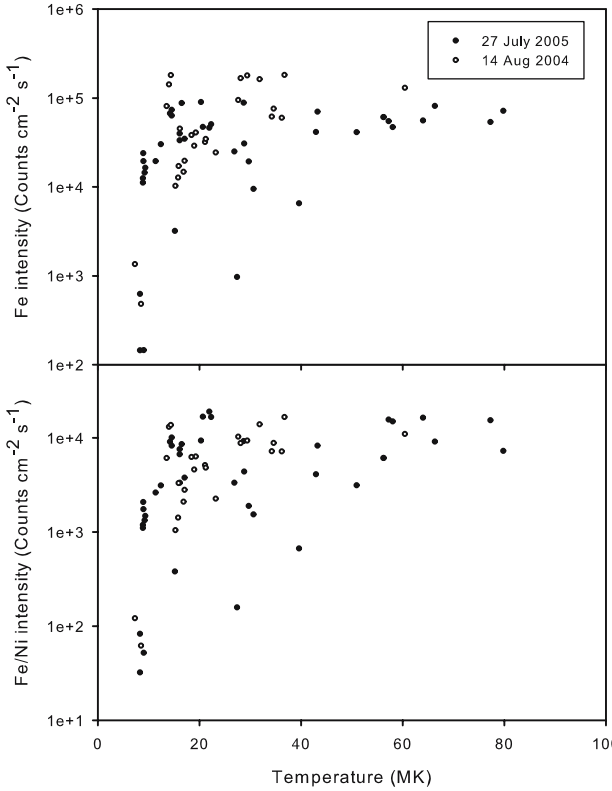

Figure 6. Integrated line intensity of Fe and Fe/Ni features as a function of temperature measured in 14 August 2004 and 27 July 2005 flares.

Hα images during rise phase varying between 10^{27} and 10^{28} cm^3 suggesting electron density (N_e) to be $> 10^{11}$ cm^{-3}. After the peak of the flare around 05:44 UT the temperature of the flare begins to grow to reach more than 70 MK in the superhot phase of the flare around 05:47 UT. The temperature falls in the decay phase. On the other hand, temperature profile of 27 July 2005 flare appears similar to count flux. However, DEM falls exponentially from 10^{49} to 10^{42} cm$^3 \cdot$keV^{-1} during rise phase of the flare and then increasing during decay phase suggesting that most of the X-ray emission is caused by heating of the plasma. The measurement of temperatures, emission measure at 2 keV, and multi-thermal power-law index by spectra fit enabled us to justify the relation (1) that DEM decreases as power-law with increase in temperature as shown in Fig. 8.

The negative power-law index below (γ_1) and above (γ_2) break energy measured from broken power-law fit of the spectrum in simultaneous to multi-thermal and line emission is shown in Fig. 9 as a function of plasma temperature (T_e). The power-law index below break energy represents thermal part of the flare spectrum and therefore it increases with temperature as may be noted from Fig. 9. On the contrary, power-law index above (γ_2) break energy representing non-thermal part of the spectrum is very high at lower temperature and decreases with T. In the case of the 14 August 2004 flare, the γ_2 was higher during rise phase in context to non-thermal onset of the flare, while it was very low in the case of 27 July 2005 flare as the onset was thermal.

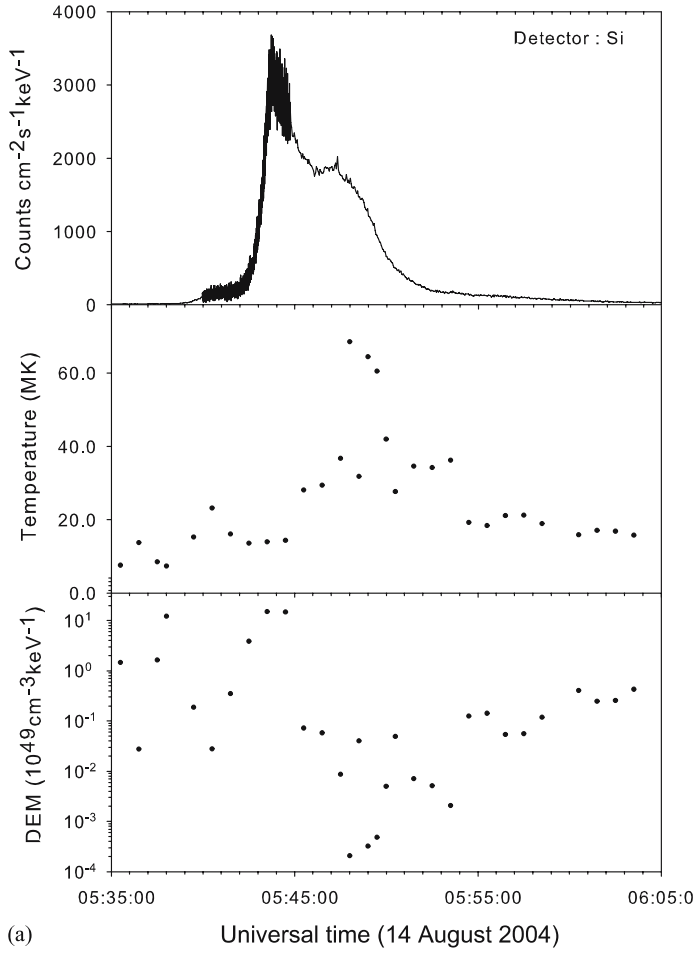

Figure 7. (*Continued*)

3.3 *Break energy*

The determination of the low-energy cut-off to nonthermal electron distributions is critical to the calculation of the nonthermal energy in solar flares. The most direct evidence for low-energy cutoffs is flattening of the power-law, nonthermal X-ray spectra at low energies. However, because of the plasma preheating often seen in flares, the thermal emissions at low energies may hide such spectral flattening of the nonthermal component. We select the 14 August 2004 and 27 July 2005 flares to estimate the break energy (cut-off energy between thermal and non-thermal emission) considering first the concept of "early impulsive flares", in which the $\geq$ 25 keV hard X-ray (HXR) flux increase is delayed by less than 30 s after the flux increase at lower energies. Thus, the plasma preheating in these flares is minimal, so the nonthermal spectrum can be determined to lower energies than in flares with significant preheating. As shown earlier in section 3.2, the flare of 14 August 2004 is impulsive in the early stage, while that of 27 July 2005 began with thermal emission. In these events, the break energy of the multi-thermal power-law and non-thermal power-law fit to the HXR spectra lies

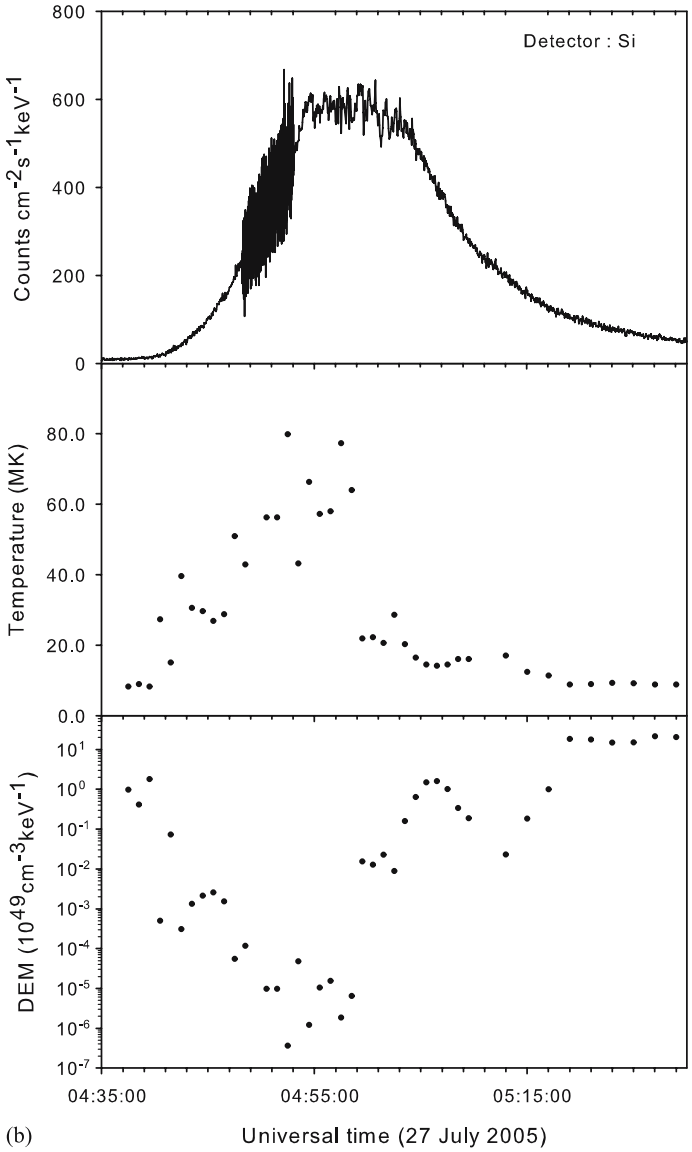

Figure 7(a & b). Variation of count flux in 10–20 keV (top panel), temperature (middle panel) and differential emission measure (bottom panel) as a function of time in the 14 August 2004 and 27 July 2005 flares.

in the range 5–20 keV, significantly lower than the value we have seen for other flares that do not show such early impulsive emissions. We show in Fig. 10 the evolution of break energy in the 14 August 2004 and 27 July 2005 flares measured from the spectra observed by Si detector with ± 0.8 keV energy resolution. It may be noted that the break energy in the 14 August 2004 flare is very low in the beginning of the flare due to non-thermal onset of the flare, and it slowly increases with time as the temperature of the flare also increases. While in the case of the 27 July 2005 flare event it is high in

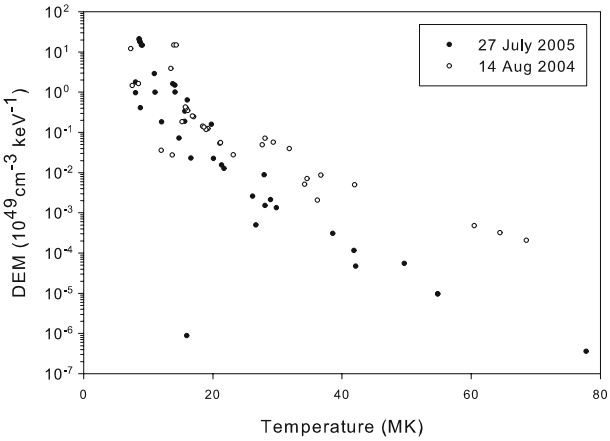

Figure 8. The differential emission measure (DEM) as a function of temperature measured in the 14 August 2004 and 27 July 2005 flares observed by Si detector of SOXS mission.

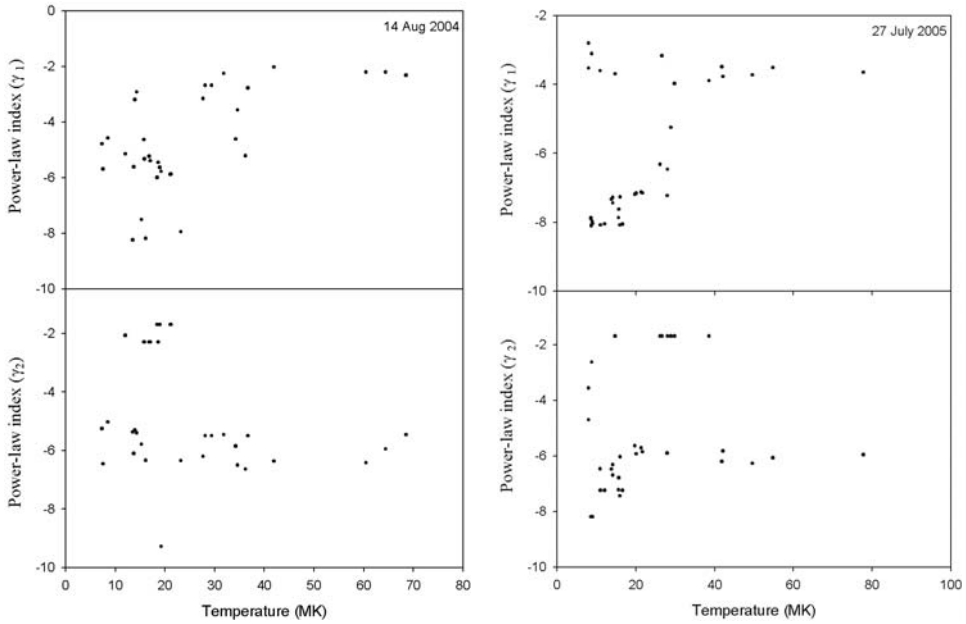

Figure 9. Variation of broken power-law index below (γ_1 – top panel) and above (γ_2 – bottom panel) break energy as a function of flare plasma temperature measured in the 14 August 2004 and 27 July 2005 flares.

the early phase due to thermal onset of the flare, however, it decreases with time as temperature goes down but electron density had already increased as revealed from high differential emission measure.

In Fig. 11 variation of break energy as a function of temperature of the flare plasma is presented. It may be noted that the break energy increases with temperature up to 40 MK. We do not have enough points above 40 MK to suggest that the break energy

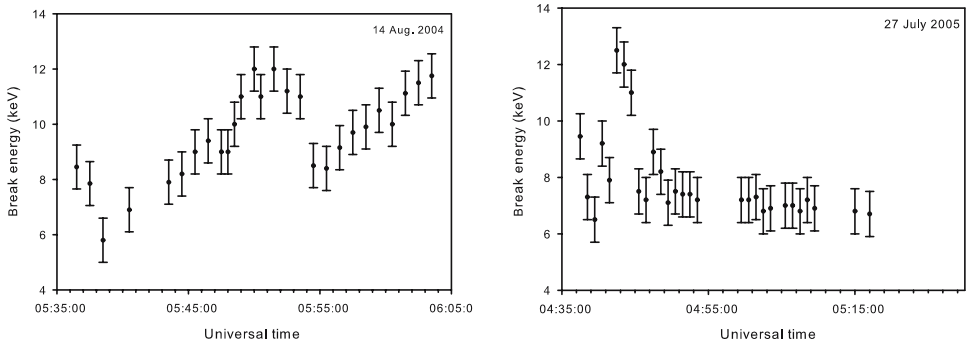

Figure 10. Break energy as a function of time measured by Si detector with 0.8 keV FWHM in the 14 August 2004 and 27 July 2005 flares.

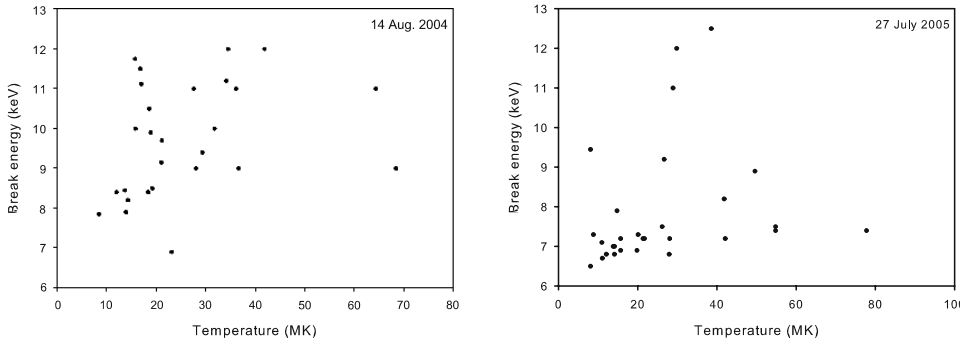

Figure 11. Break energy as a function of flare plasma temperature in the 14 August 2004 and 27 July 2005 flares. Estimation of break energy is restricted to ± 0.8 keV, resolution of the Si detector.

falls above this temperature though it appears in both flares. The increase of break energy with temperature suggests that low energy cut-off of non-thermal mechanism shifts to higher energy due to increasing contribution of thermal bremsstrahlung at higher and higher temperatures (super-hot) of the flare plasma.

3.4 *Microflares*

Solar flares propel energetic particles into space and are thought to be the main source of heat pumping the Sun's outer atmosphere to about a few million degrees Celsius. But with the investigation of small scale flares called micro and nanoflares by YOHKOH, SOHO and RHESSI it has been suggested that these tiny numerous microflares may influence solar atmosphere more than the solar flares. Now observations show that microflares a million times smaller are more frequent and may provide a major portion of the heat in the corona. The microflares are identified by their hard X-ray emission. However, there are observations of microflares being mainly thermal events, heating the Sun but not accelerating particles like larger flares (Jain *et al.* 2006c). If that were the case, they would produce more low-energy soft X-rays than high-energy hard

X-rays. Interestingly, a subset of microflares is responsible for type III radio bursts, which, however, do very little heating of the solar corona. Instead, the stream of high-speed particles they produce seems to jet unchecked out of the Sun at speeds up to one-third the speed of light, exciting radio oscillations at lower and lower frequencies as the particles pass through lower and lower density plasma. This probably has to do with the magnetic field in the region around the microflare, since particles are tied to the field lines and have to run along them, we think that for normal microflares, the particle acceleration occurs in a closed magnetic region so the electrons cannot get away; they do more heating that way. In type III bursts, the electrons are accelerated in an open magnetic field, and they have an easy way to escape, so they do some less of heating. Mirzoeva (2006) using the data from Interball–Geotail project for the period September through December 1995 derived the intensity distribution of microflares and found correlations between the daily mean peak fluxes of X-ray bursts from microflares of various classes and the daily mean values of the thermal background of the solar corona. He suggested that microflares play a significant role in heating the solar corona. Jain *et al.* (2006a) showed that the minimum temperature required for the formation of Fe and Fe/Ni line features are 8 and 14 MK respectively. In view of high Z of these elements they settle down very fast against gravitation of the Sun as soon as the temperature of the corona goes below these temperatures.

We investigate low-intensity microflares in the soft and medium hard component (4–20 keV) of the solar X-ray radiation and explore the possibility of the presence of Fe and Fe/Ni line features to probe their role in heating the corona.

Shown in Fig. 12 are the spectrograms of the microflares observed on 1 May 2004, 27 April 2007 and 3 June 2007 by Si detector, which unambiguously represent the presence of Fe line feature. In all three microflares though weak, signatures of Fe/Ni line feature are also visible further indicating that temperatures in these microflares could reach to 14 MK. Presence of these line features in microflares show their strength to heat the active region corona to 8 MK or more. On the other hand their spectra fit provide an evidence of the presence of thermal plus non-thermal components indicating heating of the plasma as well as the particle acceleration inside the magnetic loops.

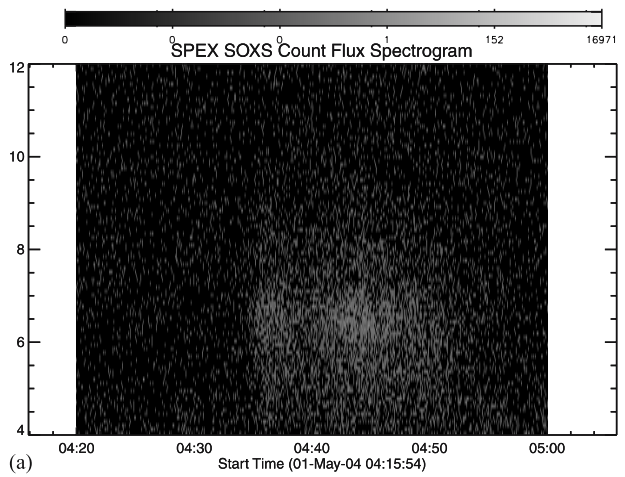

(a)

Figure 12. (*Continued*)

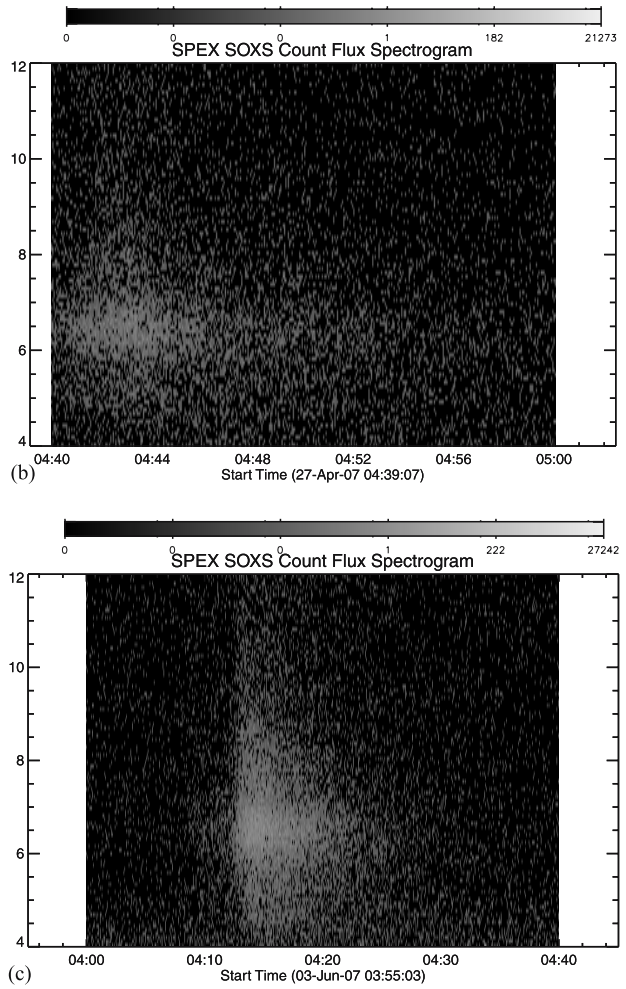

Figure 12(a–c). X-ray spectrograms of microflares observed by Si detector on 1 May 2004, 27 April and 3 June 2007. The intense Fe line feature around 6.7 keV during the flare interval may be noted in all flares, while faint signature of Fe/Ni line feature around 8 keV may also be seen in 27 April and 3 June 2007 microflares.

In Fig. 13, we show the spectra integrated over one minute during rise phase of the microflares, viz., 27 April 2007 and 3 June 2007. It may be noted that spectra of 27 April 2007 is best fitted by multi-thermal while that of 3 June 2007 by multi-thermal plus non-thermal assumptions. However, sometimes in small microflares ($<$ B5) we are not able to see the signature of Fe line feature perhaps due to the sensitivity of the detector limiting to this intensity. In future if detectors with higher sensitivity are flown then not only micro but also nanoflares may show the presence of Fe line feature, which may further emphasize the possibility of these small scale activities to be responsible for heating the solar corona.

The count flux, temperature and differential emission measure as a function of time of these three microflares under current investigation are shown in Fig. 14. It may be

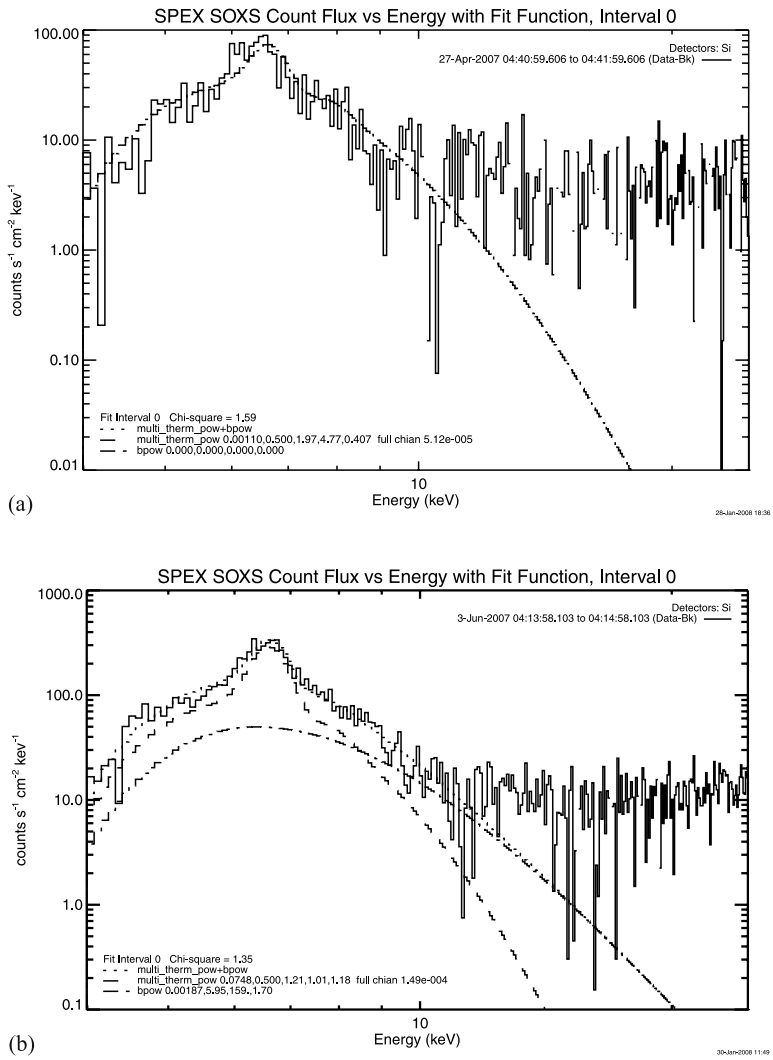

Figure 13(a & b). Count spectra fit by multi-thermal and broken power-law assumption of the 27 April and 3 June 2007 microflares during their rise phase.

noted that the microflare of 1 May 2004 is weak and slow rising while the 27 April 2007 is medium intense, and 3 June 2007 appears to be a fast rising microflare and stronger than the other two flares. Power-law inverse relationship between temperature and differential emission measure may also be observed in the microflares.

A small pre-heating was observed in the 1 May 2004 microflare during which maximum temperature was around 18 MK. The temperature decayed until 04:40 UT and then started to increase with main microflare to reach maximum about 24 MK. However, it may be noted that emission measure was very small in this microflare ranging between 10^{38} and 10^{43} cm$^{-3}\cdot$keV^{-1}. This suggests that neither particle acceleration nor the ionization of the plasma was the case in this microflare, rather simple heating of the ambient plasma by increased temperature appears be more appropriate. On

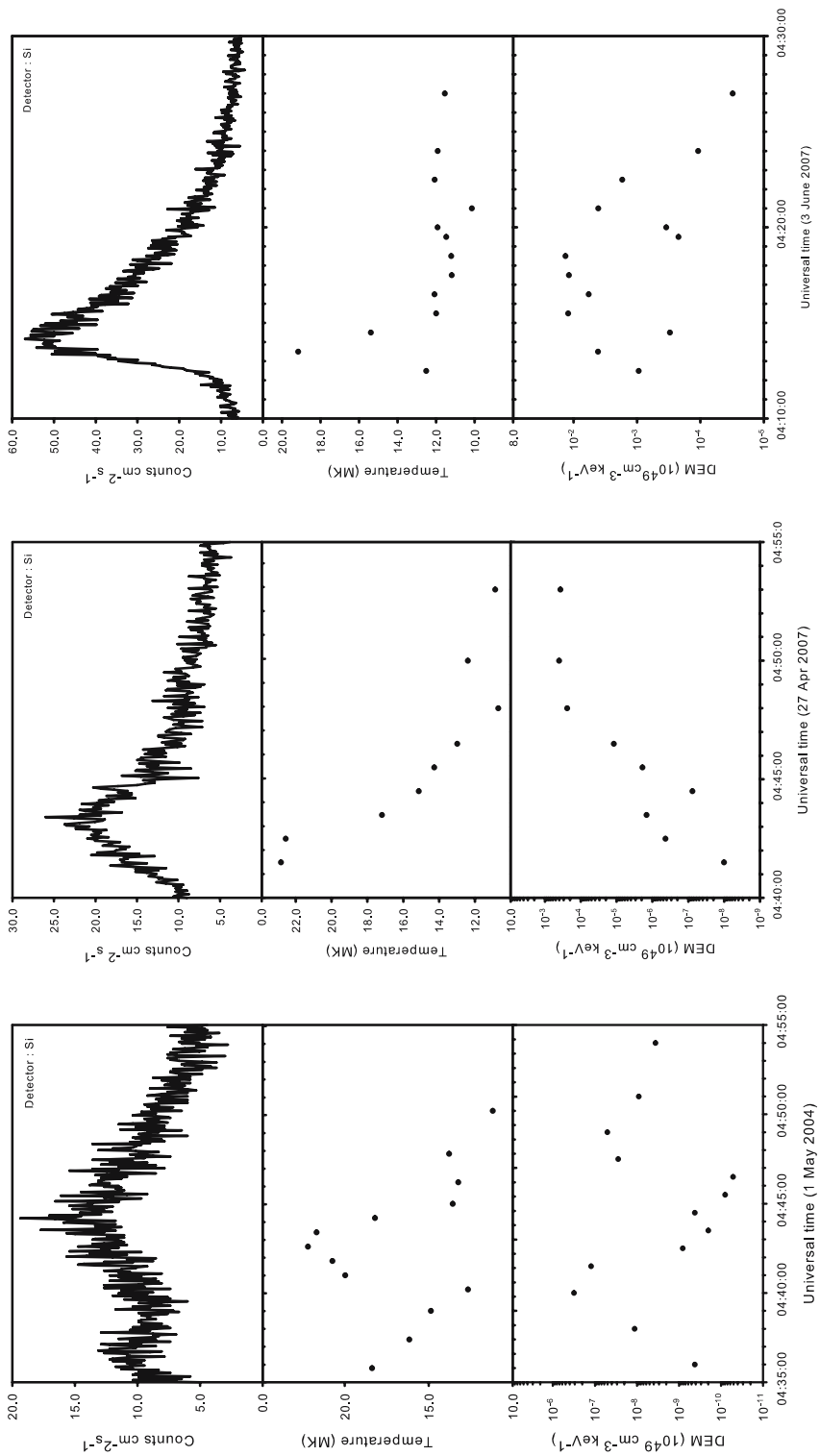

Figure 14. Variation of X-ray count flux, temperature and emission measure of flare plasma as a function of time in 1 May 2004, 27 April 2007 and 3 June 2007 microflares.

the other hand the case of 27 April 2007 microflare ionization by heating or particle acceleration in the closed loop structure appears as a suitable case in context to power-law increasing of emission measure from 10^{41} to $10^{46}\,\mathrm{cm}^{-3}\cdot\mathrm{keV}^{-1}$ with decrease of temperature. The case of 3 June 2007, however, appears to us of hybrid configuration where plasma heating by both temperature and particle acceleration was in the progress as may be noted from the thermal and non-thermal fit of the spectra shown in Fig. 14(b). The emission measure was observed to range between 10^{44} and $10^{47}\,\mathrm{cm}^{-3}\cdot\mathrm{keV}^{-1}$, significantly higher than the other two microflares.

No signature of type III radio bursts were observed in association to these flares. Thus it appears that the magnetic reconnection was in closed loop structure in the lower corona or transition region causing heat by thermal as well as by accelerated particles, which thermalized during their gyration along the loops. However, recently Aschwanden (2007) showed that the energy released by microflares/nanoflares in the corona is not enough to heat the corona. He suggested that if such small scale flares are considered to heating upper chromosphere and/or transition region then they may also play a significant role in coronal heating.

4. Discussions and conclusions

In the current analysis of SOXS flare data, the spectra in the dynamic energy range 4–23 keV during flare interval were analyzed considering line Gaussian, multi-thermal power-law and broken power-law functions to fit the Fe-line and Fe/Ni-line features with Gaussian profiles at 6.7 keV, and $\sim$ 8 keV respectively, and thermal and non-thermal spectra consisting of a continuum (free-free plus free-bound emission). The data analysis was performed using OSPEX/SolarSoft package that accounts for all known instrumental effects and allows for background subtraction. The multi-thermal power-law was used in view of varying emission measure as a function of temperature, in addition to line Gaussian and broken power-law to fit the spectra. The fits to the model spectra are most reliable for Si detector's spectra taken during the flares (as measured by the reduced χ^2).

Phillips *et al.* (2006) and Jain *et al.* (2006b) showed that the observed equivalent widths (w) of Fe line feature increase with T_e more sharply than is predicted by the theoretical curve, with a clear displacement to higher temperatures being indicated. These results are not so easily explained. If the isothermal approximation is a good one for spectra during these flares, as is indicated by the reduced χ^2 values, then possibly this behaviour could indicate the need for a correction to the ionization fractions of Mazzotta *et al.* (1998). This suggests to differential emission measure indicating to multi-temperature model instead of single temperature approximation that was considered so far in the X-ray spectral analysis of the flares. In this investigation intensity of the Fe and Fe/Ni line features was found to increase with temperature up to 45 MK. However, beyond 45 MK increase or decrease was not clear due to limited observations. Thus we propose to analyze more flares of similar intensity and by the same techniques to investigate behaviour of line intensity above 45 MK.

We found that 14 August 2004 flare started as non-thermal mechanism while 27 July 2005 as plasma heating process. However, the differential emission measure shows power-law decrease as a function of the flare plasma temperature (T_e). This was confirmed by break energy, which increases with temperature, as well as by the variation of spectral index (γ_1) below breaks energy, which is representative of free-free

continuum thermal bremsstrahlung emission, and increase with temperature. On the other hand the spectral index γ_2, above break energy, representative of free-bound continuum, i.e., non-thermal emission reduces with temperature.

We found the signatures of Fe and Fe/Ni line features in microflares of varied intensity indicating flare plasma temperatures exceeding 14 MK required to form Fe and Fe/Ni line features. Their spectra analysis unambiguously showed temperatures more than 20 MK, and particle acceleration, however, apparently in closed loop configuration. Based on the evidence of line features and spectra fit by multi-thermal and broken power-laws we conjecture hybrid model for microflares with thermal plus non-thermal mechanisms. Incidentally, the energy released by such microflares is not found sufficient to heat the active region corona (Aschwanden 2007). However, the absence of type III radio bursts in association with the microflares studied by us indicate that they had very small and closed loops, and therefore originated either in upper chromosphere or in transition region where the "tectonic" photospheric random motion driven by subphotospheric convection is likely to cause small-scale reconnection processes in the transition region (Priest *et al.* 2002), which heat up the plasma at the footpoints of coronal loops and fill them up subsequently. Recent hydrodynamic simulations by Warren *et al.* (2002, 2003) employ an intermittent heating process localized at the loop footpoints, which produces a sequence of repeated heating pulses that are able to mimic the observed temperature evolution of coronal loops. As soon as the overpressure starts to fill up the loop with hot plasma, the loop is expected to brighten rapidly in the soft X-rays first (during a filling-time interval that is in the order of a shock loop-crossing time, i.e., within minutes for typical coronal loops), without any detectable signal in the cooler EUV channels. Consequently, we would observe only the cooling phase, when the loop cools down from the soft X-rays through EUV. Such loop cooling phases from *Yohkoh* soft X-ray filters down to *TRACE* EUV filters have indeed been observed in detail for 11 cases, over time intervals of several hours, without any noticeable EUV signature of an initial heating phase (Winebarger & Warren 2005; Ugarte-Urra *et al.* 2006). The footpoint of a loop has been monitored in EUV during the initial rise in soft X-rays in detail in a single case (Fig. 6 in Ugarte-Urra *et al.* 2006), but the full loop was not detected in EUV ($T = 1.0$–1.5 MK) until it cooled down from the hotter ($T = 3.8$ MK) soft X-ray temperatures. Caveats of the "chromospheric evaporation scenario" for heating of quiescent loops are:

- the non-detection of the initial heating agent (small-scale reconnection events in the transition region) and
- the lack of observed blue-shifted upflows, which are probably to blame on insufficient time cadence, spatial, and spectral resolution.

We propose that plasma heating resulting from nanoflares and microflare events occurs in the transition region, rather than throughout the corona in higher altitudes. Recent imaging observations of EUV nanoflares and soft X-ray transient brightenings invariably show small-scale loops with length scales of $L = 2000$–3000 km that barely stick out of the transition region (Aschwanden & Parnell 2002). In the model of Parker (1988), where coronal field lines are more or less uniformly twisted along their lengths, heated plasma would spread along the coronal field lines and would manifest itself in long (probably unresolved) thin threads, for which we have no observational evidence. Thus we see strong support for the working hypothesis that the major heating

source responsible for a hot corona is located in the transition region rather than in the corona.

Acknowledgements

We are grateful to Prof. Brian R. Dennis and Dr. Richard Schwartz for providing the OSPEX software and many fruitful discussions on its application and data analysis techniques. Authors are also thankful to Prof. K. J. H. Phillips for extensive scientific discussion on this investigation related to Fe and Fe/Ni line features. We express our special thanks to Mr. K. J. Shah and Mrs. Jayshree Trivedi for helping us in preparing figures for this investigation. Anonymous referees deserve our sincere thanks for suggesting this better presentation of the current investigation. The synoptic observations from SOXS payload onboard GSAT-2 spacecraft are provided by ISRO and being archived at PRL.

References

Aschwanden, M. J., Parnell, C. E. 2002, *ApJ*, **572**, 1048.
Aschwanden, M. J. 2007, *ApJ*, **659**, 1673.
Dere, K. P., Landi, E., Mason, H. E., Monsignori Fossi, B. C., Young, P. R. 1997, *Astron. Astrophys.*, **125**, 149.
Jain, R., Rao, A. R., Deshpande, M. R., Dwivedi, B. N., Manoharan, P. K., Seetha, S., Vahia, M. N., Vats, H. O., Venkatkrishnan, P. 2000a, *Bull. Astron. Soc. India*, **29**, 117.
Jain, R., Deshpande, M. R., Dave, H. H., Manian, K. S. B., Vadher, N. M., Shah, A. B., Ubale, G. P., Mecwan, G. A., Trivedi, J. M., Solanki, C. M., Shah, V. M., Patel, V. D., Kayasth, S. L., Sharma, M. R., Umapathy, C. N., Kulkarni, R., Kumar, Jain, A. K., Sreekumar, P. 2000b, Technical Document – *GSAT-2 Spacecraft – Preliminary Design Review (PDR) Document for Solar X-ray Spectrometer,* ISRO-ISAC-GSAT-2-RR-0155, Bangalore, Published by Indian Space Research Organisation.
Jain, R., Dave, H. H., Shah, A. B., Vadher, N. M., Shah, V. M., Ubale, G. P., Manian, K. S. B., Solanki, C. M., Shah, K. J., Kumar, Sumit, Kayasth, S. L., Patel, V. D., Trivedi, J. J., Deshpande, M. R. 2005, *Solar Phys.*, **227**, 89.
Jain, Rajmal, Pradhan, Anil K., Joshi, Vishal, Shah, K. J., Trivedi, Jayshree, J., Kayasth, S. L., Shah, Vishal M., Deshpande, M. R. 2006a, *Solar Phys.*, **239(1–2)**, 217–237.
Jain, Rajmal, Joshi, Vishal, Kayasth, S. L., Dave, Hemant, Deshpande, M. R. 2006b, *J. Astrophys. Astron.*, **27(2 & 3)**, 175–192.
Jain, Rajmal, Joshi, Vishal, Hanaoka, Yoichiro, Sakurai, T., Upadhyay, Nipa 2006c, *J. Astrophys. Astron.*, **27(2 & 3)**, 339–346.
Mazzotta, P., Mazzitelli, G., Colafrancesco, S., Vittorio, N. 1998, *Astron. Astrophys. Suppl.*, **133**, 403–409.
Mirzoeva, I. K. 2006, *Astronomy Letters*, **32(1)**, 69–72.
Parker, E. N. 1988, *ApJ*, **330**, 474.
Phillips, K. J. H. 2004, *ApJ*, **605(2)**, 921–930.
Phillips, K. J. H., Rainnie, J. A., Harra, L. K., Dubau, J., Keenan, F. P., Peacock, N. J. 2004, *Astron. Astrophys.*, **416**, 765–773.
Phillips, K. J. H., Chifor, C., Dennis, B. R. 2006, *ApJ*, **647(2)**, 1480–1490.
Priest, E. R., Heyvaerts, J. F., Title, A. M. 2002, *ApJ*, **576**, 533.
Ugarte-Urra, I., Winebarger, A., Warren, H. P. 2006, *ApJ*, **643**, 1245.
Warren, H. P., Winebarger, A. R., Hamilton, P. S. 2002, *ApJ*, **579**, L41.
Warren, H. P., Winebarger, A. R., Mariska, J. T. 2003, *ApJ*, **593**, 1174.
Winebarger, A. R., Warren, H. P. 2005, *ApJ*, **626**, 543.